Chapter 9
Flowslide Investigations Test Rig Design

Giandomenico Di Massa, Luca Pagano, Stefano Pagano, Michele Russo, Riccardo Russo, and Maria Claudia Zingariello

Abstract The paper describes a mechanical slope developed to investigate rainfall-induced shallow landslides in loose coarse-grained soils, which can evolve into high-speed flowslides with propagation capabilities even in areas with very low gradients, putting people's lives and property at risk. The mechanical slope is the main component of an experimental plant built at the University of Naples. It consists of two inclinable parts: the upper one where the soil sample is deposited and the flowslide is generated, and the lower part that allows flowslide behaviour to be observed. The monitoring system implemented consist of load cells which measure the sample weight changes, tensiometers and Time Domain Reflectometry (TDR), which measure, respectively, soil suction and water content at different depths, Particle Image Velocimetry (PIV) and a Laser scanner techniques which provide the sample surface movements.

Keywords Instrumentation • Mechanical simulation • Physical model • Rainfall-induced landslides • Test rig • Two link mechanism

1 Introduction

Natural slopes in loose soils are often subject to wetting-induced instabilities involving shallow layers [1, 2]. These phenomena frequently pose hazards due to their rapid kinematics, especially when the soil grain-size distribution lies between that of gravelly sands at coarsest and sandy-silt at finest [3]. In this grain-size range capillarity effects are significant, with resulting suction levels being suitable for contributing to slope stability [4–7]. Instability upon wetting is usually induced by

G. Di Massa • S. Pagano (✉) • M. Russo • R. Russo
Dipartimento di Ingegneria Industriale, Università degli Studi di Napoli Federico II, via Claudio n. 21, Naples 80125, Italy
e-mail: stefano.pagano@unina.it

L. Pagano • M.C. Zingariello
Dipartimento di Ingegneria Civile, Edile e Ambientale, Università degli Studi di Napoli Federico II, via Claudio n. 21, Naples 80125, Italy

© Springer Science+Business Media Dordrecht 2015

G.-C. Yang et al. (eds.), *Transactions on Engineering Technologies*,
DOI 10.1007/978-94-017-9804-4_9

rainfall [8, 9], even if there may be other contributory factors, such as water lost from hidden underground conduits or water infiltration generated by human activities.

Precipitation events causing instabilities may vary according to the soil type involved. Highly pervious slopes made of gravelly sands become unstable under the effects of very intense, usually short-lasting, precipitation, without any effect exerted by antecedent rainfall. On the other hand, slopes in sandy-silty soils lose stability under the effects of prolonged wet periods followed by a major event of significant intensity [3, 8, 10].

In order to investigate what relationship establishes between precipitation history and landslide triggering under different conditions involving soil types, soil states (essentially porosity), slope inclination and slope thicknesses, a physical model was built. It consists of a mechanical slope with adjustable inclination and with the possibility of controlling or measuring the main factors that contribute to triggering a landslide. The paper presents the design of the prototype, describes its main mechanical features and shows its flexibility in changing slope factors.

2 Soil Sample Cycle

The plant consists essentially of a variable inclination mechanical slope and of other components that allow the soil sample to be reused for the execution of other tests [11]. The sample cyclically executes the following path (Fig. 9.1). It is deposited on the upper part (Part-A) of the mechanical slope (Figs. 9.2 and 9.3) by means of a hopper which moves slowly (0.2–8 cm/s) at a constant distance from Part-A. The material flows through an adjustable slit placed at the bottom of the hopper. The height of the hopper can be regulated to take account of the properties of the material to be deposited and the desired degree of compaction.

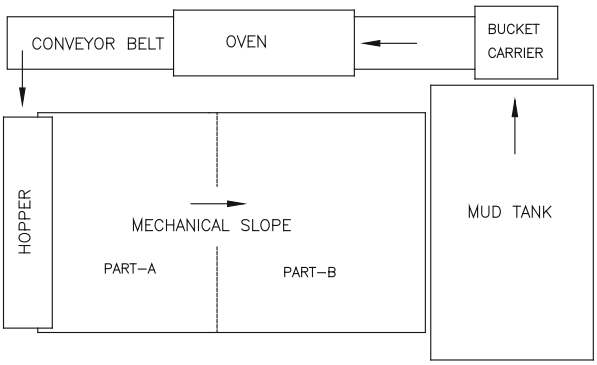

Fig. 9.1 Plant scheme and sample cycle

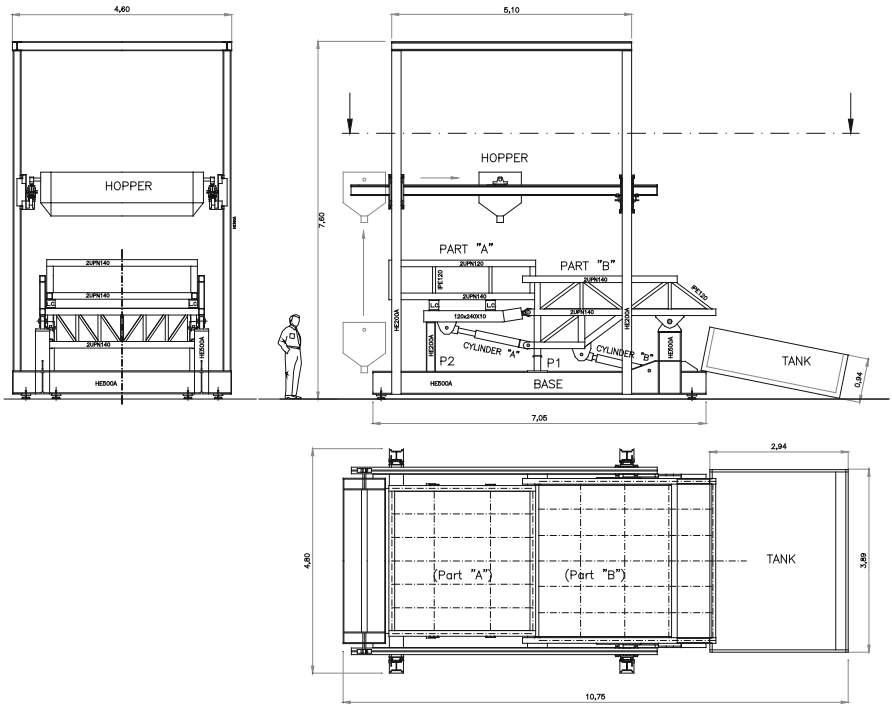

Fig. 9.2 Mechanical slope and deposition system

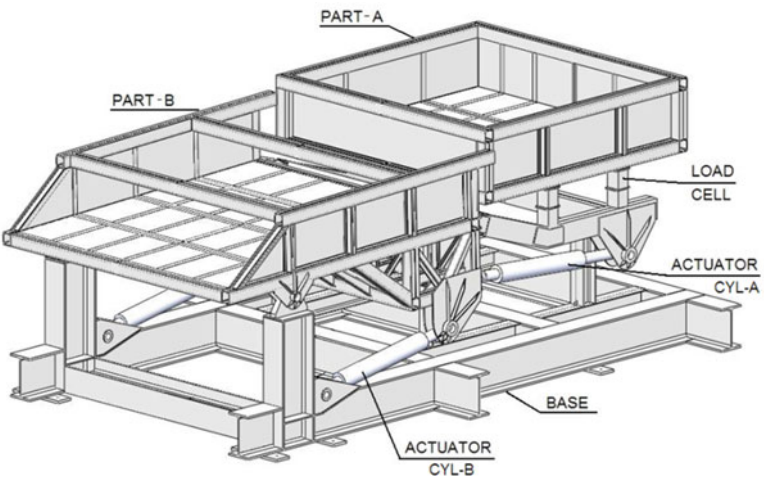

Fig. 9.3 Mechanical slope

The mechanical slope can be tilted after or before the deposition step; in the first case the hopper translates onto tilted guides, parallel to part-A, in order to keep the distance between the hopper and part-A constant (Fig. 9.4).

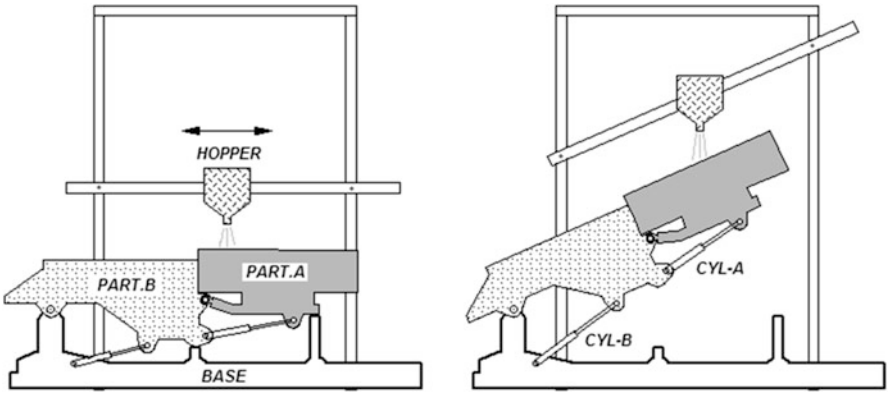

Fig. 9.4 Deposition phase

After the deposition phase the sample is subjected to artificial rainfall until it collapses. Then the collapsed soil flows onto Part-B and is collected in the mud tank. From this tank, the sample is raised, by means of a bucket carrier, onto a conveyor belt and is transported into a passing oven where the sample is dried. Then the sample can be re-deposited on part-A for a new test.

3 The Mechanical Slope

The mechanical slope consists of a base on which is articulated a two-link-mechanism; the two moving parts have the following plan dimensions (Fig. 9.3): Part-A, 3 × 3 m; Part-B, 4 × 3 m.

Part-A is instrumented to measure the weight changes of the sample. Both parts have side walls 0.70 m high to confine the sample under test. Their frames are made of steel beams (mainly wide flange beams and channel section shapes) joined by welding. The base is made of two principal horizontal H-section beams (HE500A) 7.10 m wide, connected crosswise by four other H-section beams.

Onto the base the following are welded:

- Two pillars (HE500A) on which part-B is pin-connected;
- The supports for the two lower hydraulic cylinders (cyl-B);
- Two pairs of H-section pillars, P1 and P2 (Fig. 9.2), placed under part-B and part-A respectively, to sustain the mechanical slope at rest in the horizontal configuration;
- The support for the columns of the frame sustaining the moving hopper.

Part-A and part-B are built with rectangular hollow section beams, obtained by welding two U-shaped beams (UPN140 or UPN120); the bottom and side walls of both parts are coated with 6 mm-thick steel plates.

The base and part-B are hinged with two steel pivots (ϕ95) and rolling bearings. Part-A is connected to part-B by means of two spherical joints and can be tilted with respect to part-B by using two hydraulic cylinders (Cyl-A).

Four load cells (Fig. 9.3) are interposed between the tank of part-A its supporting frame to measure the changes in sample weight due to the water absorbed during a test.

By powering the lower cylinders (Cyl-B) the entire mechanical slope can be tilted, with respect to the horizontal, up to 45°; the other pair of cylinders (Cyl-A) allows part-A to be tilted with respect to part-B in the range: +15°; −45°. The maximum inclination speed of the two elements is approximately 0.1°/s.

To define the cylinder thrust and the power required to lift the slope, the symmetry of the system was considered and one-half of the mechanical slope was analysed.

The following overall masses are considered:

– Part-A, including the load cells and the upper cylinders: 2,400 kg;
– Part-B, including the lower cylinders: 2,800 kg;
– soil sample on part-A: 12,600 kg.

The maximum thrust exerted by the cylinders and the forces acting in the pin joints connecting the slope elements were evaluated for different configurations of the mechanical slope.

Figure 9.5 reports the thrust required to tilt the slope up to 45°. The thrust has its maximum value, equal to about 300kN, when the mechanical slope is horizontal. The same figure reports the force acting in the pinned connection with the base.

Figure 9.6 reports the thrust required for the upper cylinders and the force in the pin connection between the two parts; the diagram considers the absolute part-A rotation ranging in the interval 0–50°, with part-B tilted by 45°. Even in this case the thrust reaches its maximum value when part A is in the horizontal position; in this configuration the thrust arm, with respect to the pin joint, is minimal.

The mechanical slope is tilted by means of two pairs of single-rod hydraulic cylinders [12, 13] (Bosch Rexroth - mod. CDM1); the lower ones (cyl-B) have a bore of 160 mm and a piston rod diameter of 110 mm; the maximum thrust is equal to 344 kN with an oil pressure of 170 bar. The upper cylinders (cyl-A) have a bore of 125 mm and piston rod diameter of 90 mm and can exert a thrust of 211 kN at 170 bar. The two pairs of cylinders are powered by the same oil pump with 22 cm^3 of displacement and maximum flow rate of 32 l/min; the pump is driven by an 11 kW electric motor. Synchronization between each pair of cylinders is guaranteed by the mechanical connections and by the flow divider valves that provide the same oil flow from the single source into the two actuators.

4 The Hopper

The hopper (Figs. 9.2 and 9.10) is made of sheet steel and is supported by two ϕ80 pins, engaged on two sliders guided on two beams. The sliders allow the hopper to

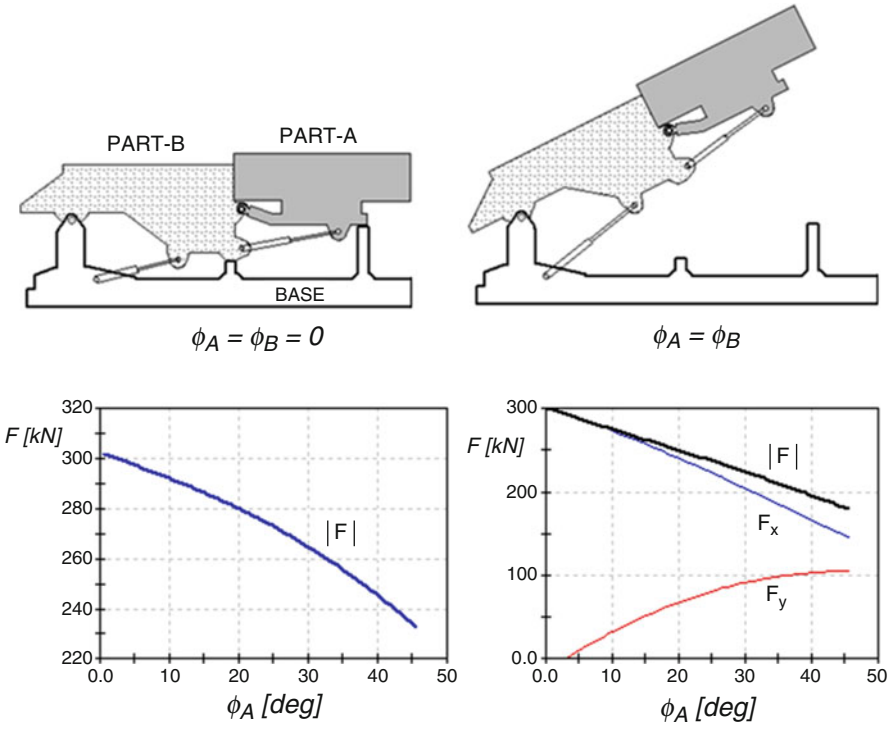

Fig. 9.5 Cylinder-A thrust and force acting in the pinned connection with the base (horizontal, Fx, and vertical, Fy, components)

translate, forward and backward, along the supporting beams during the deposition step; the translating movement is driven by two electric motors and two lead-screw systems.

The two sustaining pin axes are displaced above the hopper centre of mass such that the hopper always assumes the same vertical orientation even when the supported beams are inclined.

The two beams can climb the four columns to adjust the hopper height to achieve the suitable distance from part-A; they can also rotate to adapt the inclination to that of part-A. The vertical translational motion is driven by four electrical motors placed on the vertical sliders; each motor has a gear-wheel spliced on the motor shaft, engaged with a toothed rack welded on the column (Figs. 9.8 and 9.9).

The hopper has a volume of about 1.5 m^3 and can be loaded with a mass soil sample of about 3,000 kg. The whole sample can thus be deposited in several successive stages.

The amplitude of the opening can be regulated and, in order to facilitate soil exit, four mechanical vibrators are fixed on the hopper's external surface.

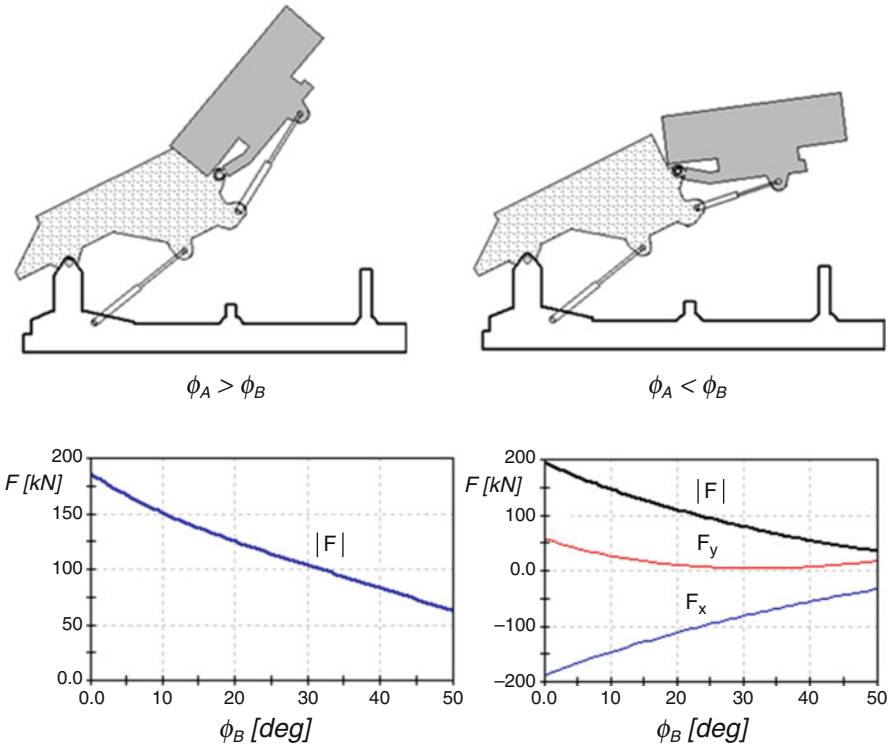

Fig. 9.6 Cylinder-B thrust and force acting in the pin connection with part-B (horizontal, Fx, and vertical, Fy, components)

5 Mechanical Slope Stress Analysis

The mechanical slope was modelled with a FEM code to perform linear static analysis and buckling linear analysis.

Figure 9.11 shows the mechanical slope in the lowest configuration, corresponding to the beginning of the lifting stage, subjected to the structural weight and sample weight of 126 kN distributed on the part-A surface. The wind action was not considered because the plant was set up inside a laboratory. This configuration, as shown in Figs. 9.5 and 9.6, involves the maximum thrusts of the hydraulic cylinders.

The main elements of the structure were modelled by linear beam element, with six degrees of freedom; the four hydraulic cylinders were instead modelled as rods, because of their terminal spherical hinges connections. Finally part-A and part-B inner linings, made of steel sheets, were modelled by means of bi-dimensional elements having membrane and bending behaviour. The base is vertically constrained in correspondence of the levelling feet (Fig. 9.7). The model

Fig. 9.7 Mechanical slope under construction: the connection between the base and part-B and the lower cylinders can be clearly distinguished. The base is supported by adjustable feet

Fig. 9.8 Mechanical slope back view. The load cells are placed between part-A tank and its supporting frame. The cylinder placed between part-A and part-B can also be seen

has about 3,000 degree of freedoms. Interpretation and consistency of the results were checked by means of simplified bi-dimensional schemes.

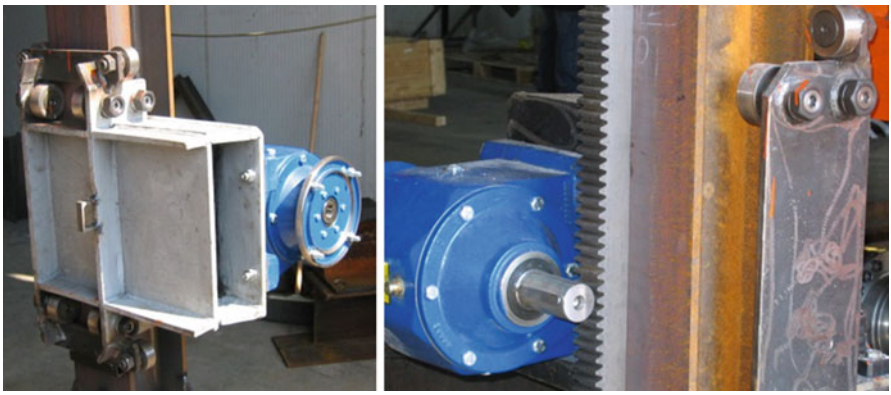

Fig. 9.9 The vertical slider allows the hopper to climb the column on which a toothed rack is welded (in the photo the gear-wheel is not yet spliced on the motor shaft)

Fig. 9.10 The hopper

Figure 9.11 shows the FEM model and the coloured map of the vertical displacement; Fig. 9.12 reports the fibre stress representation (combined axial and bending stresses) of the main elements.

6 The Instrumentation

The mechanical slope is equipped with a control/acquisition systems to govern the hydraulic actuators and to detect the instrumentation signals that allows to follow the evolution of the sample characteristics induced by the rain [14].

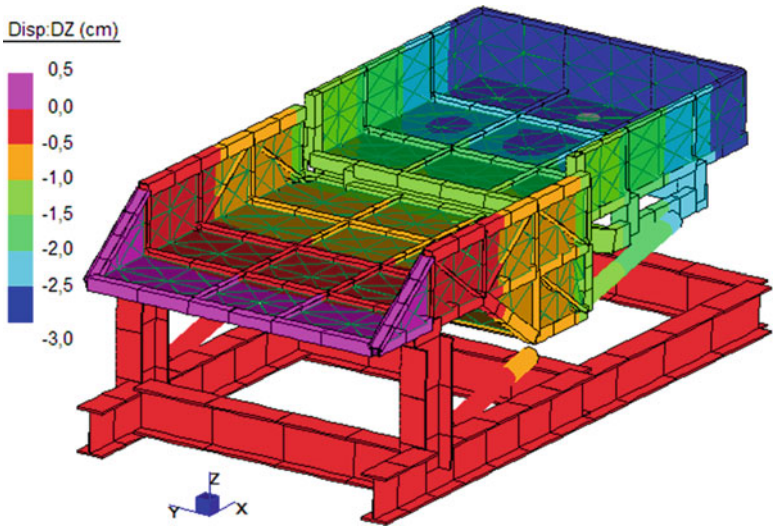

Fig. 9.11 Mechanical slope FEM model

As stated above, four load cells (MTI Multi-Component Transducers MC8-6-20000) are installed between the frame and the tank of part-A (Fig. 9.3). Each cell measures continuously in time the six reaction force components; as a result, changes in weight of part A may be obtained; such changes may be used to derive the sample unit weight during soil deposition, the changes in the water mass stored by the sample during the test (as a result of rain, seepage processes and run off), and the losses of soil mass associated to the occurrence of landslides or limited earth flows.

Once the deposition phase had been completed, the sample was wetted for about a week to reduce suction until the suction level targeted at the beginning of the test had been reached. The test was then performed tilting part-B by 30° with respect to the base and part-A by 40°. Part-A and Part-B inclination time histories are controlled by means of linear position transducers integrated in the hydraulic cylinders; tilting angles can be also checked through two removable clinometers or accelerometers.

This mechanical slope configuration makes it easier to identify post-failure behaviour by maximizing differences in time needed to cover the trench between a rapid flowslide and a slow-drying one. Rainfall intensity was assigned equal to 30 mm/h.

Increments in weight of the sample during the test indicate that the sample stores water. Importantly, the small drops in weight correspond to water lost in run-off from the sample surface and the emptying of tubes when rainfall has been stopped in order to facilitate working with the laser scanner, as explained below.

Water storage capability under constant rainfall intensity however declines with time, as indicated by the decrease in the derivative of the curve. This reduction

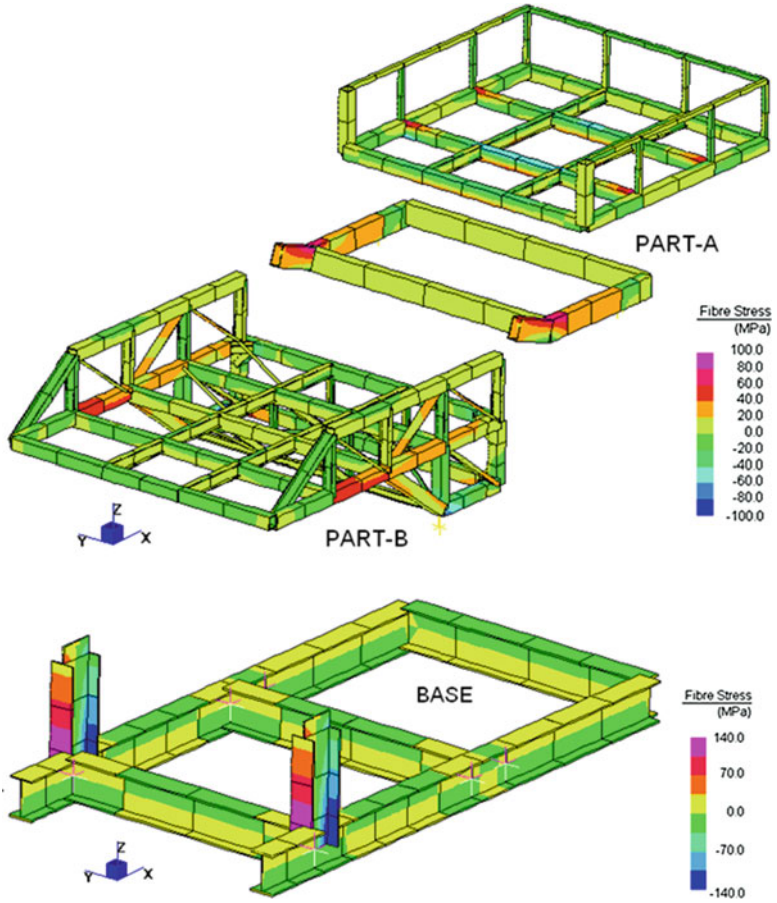

Fig. 9.12 Fibre stress representation of the main groups of elements

lowers the hydraulic gradients (driving the water drops within the sample), acting at the top surface between the exterior and interior of the sample. In the initial stages, an additional contribution to the same effect is provided by the time needed for the seeping water to reach the draining boundary downstream. Soil permeability is known to increase during the wetting process. In the initial stages, while the water has not yet drained through the permeable boundary, soil permeability increments should enhance water adsorption.

However, Fig. 9.13 indicates that permeability effects are not as substantial as those produced by the gradient reductions. Consistent with what is expressed by Fig. 9.13, initially the rainfall appears to the naked eye to be fully absorbed by the sample surface and, then increasingly rejected by it, with run-off being enhanced.

The mechanical slope is also equipped with a digital laser scanner to detect, over time, the position of the sample surface, moved by a robotized system above the

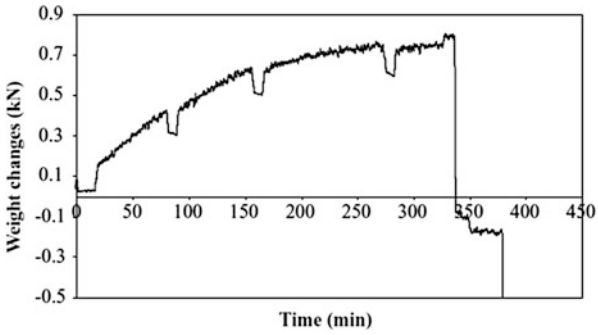

Fig. 9.13 Sample weight changes

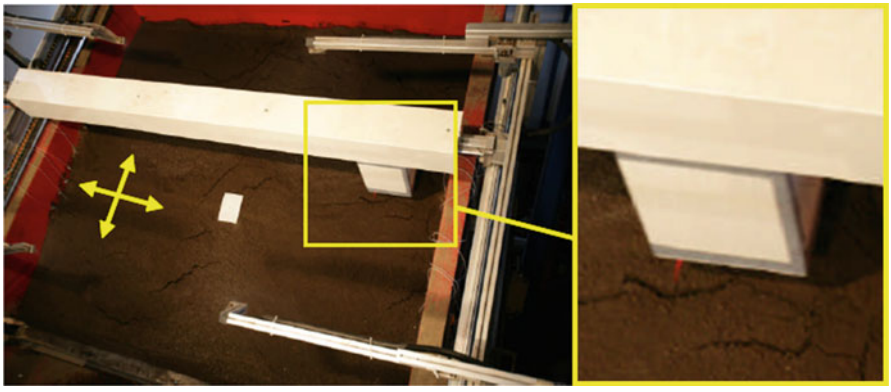

Fig. 9.14 Laser scanner apparatus on part-A

sample surface, in a plane parallel to part-A. The robotized system consists of a bar driven longitudinally by an electrical motor along two slide guides fixed on part-A border (Fig. 9.14). Another electrical motor moves the scanner transversally, along the bar.

To be strictly, the instrument generates a band of laser rays forming longitudinally on the impacted surface strip of points which are detected by the CCD sensor. Each strip is made of a large number of monitored points, being the point resolution of 0.25 mm, and is about 100 mm large.

The laser scanner sensor has a working depth ranging from $z = 120$ to $z = 220$ mm.

To determine the sample surface displacement and velocity, a video acquisition system is employed and the data of interest are derived through the Particle Image Velocimetry (P.I.V.) analysis that compares different frames at two different instant of time.

The system consists of a video camera (Basler A404K), having a pixel resolution of 0.8 Megapixel and a sample period up to 25 frames per second. The videocamera points perpendicularly to the sample surface three meters far from it (Fig. 9.15).

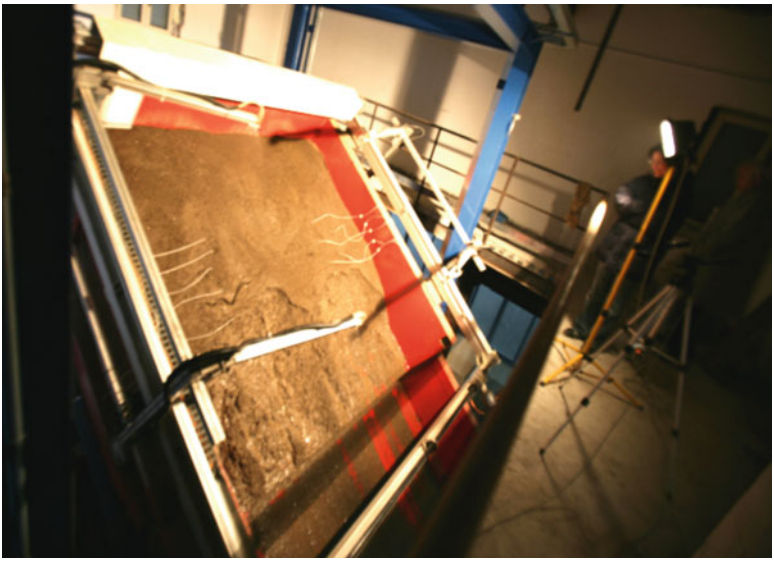

Fig. 9.15 P.I.V. apparatus

The technique enable one to individuate exactly the triggering time and to follow the kinematics of the landslide. However, the accuracy in terms of displacements, of about 2 cm, may be considered satisfactorily only for large mass movements characterizing the post-failure stages.

Finally, a number of tensiometers [15] and of TDR rod-probes [16] have been adopted to measure within the sample soil suction and water content, respectively.

For pyroclastic soils suction may be measured quite reliably through the small tip tensiometers developed by the *Soil Moisture*, since hardly suction values exceed 80 kPa, i.e. the full scale of such devices. These devices however suffer of time lag problems for high suction values. The greater the suction value the longer is the time needed for the tensiometer to equilibrate a change in suction. The time lag arises significant when suction exceeds 30 kPa, while becomes satisfactorily short below this value.

As well known, the TDR technique adopts the measurement of the soil permittivity (dielectric constant) to derive the soil water content. Soil permittivity is obtained by measuring the travel time of an electrical pulse generated by a reflectometer within a cable connected to a metallic probe inserted within the soil. The TDR device used in this experimentation is the TDR100 reflectometer developed by *Campbell* connected with 8 m long cables to a number of TDR 3-rod probes, each one 30 cm long.

Both tensiometer and TDR measurements have been acquired through a data logger (*Campebell Scientific* CR1000).

Small tip tensiometers and TDR probes have been installed within the sample during the deposition process at three or four different depths.

7 Conclusions

In this paper, a mechanical slope that allows to simulate rainfall-induced flowslides and its instrumentation useful for the measurement of the main variables involving the phenomenon was presented.

It was explained how the device allows the main factors affecting such phenomena to be taken into account. The result of a test regarding the measure of the amount of water absorbed is reported together with possible experimental procedures that may be adopted to perform the tests.

References

1. Toll, D.G., Lorenco, S.D.N., Mendes, J., Gallipoli, D., Evans, F.D., Augarde, C.E., Cui, Y.J., Tang, A.M., Rojas Vidovic, J.C., Pagano, L., Mancuso, C., Zigariello, C., Tarantino, A.: Soil suction monitoring for landslides and slopes. Quart. J. Eng. Geol. Hydrogeol. **44**(1), 23–33 (2011). doi:10.1144/1470-9236/09-010
2. Pagano, L., Zingariello, M.C., Vinale, F.: A large physical model to simulate flow-slides in pyroclastic soils. 1st European Conference on Unsaturated Soils, 1–4 luglio 2008, pp. 205–213, Durham (2008)
3. Pagano, L., Picarelli, L., Rianna, G., Urciuoli, G.: A simple numerical procedure for timely prediction of precipitation-induced landslides in unsaturated pyroclastic soils. Landslide **7**(3), 273–289 (2010). doi:10.1007/s10346-010-0216-x
4. Rianna, G., Pagano, L., Urciuoli, G.: Rainfall patterns triggering shallow flowslides in pyroclastic soils. Eng. Geol. **174**, 22–35 (2014)
5. Rianna, G., Pagano, L., Urciuoli, G.: Investigation of soil-atmosphere interaction in pyroclastic soils. J. Hydrol. **510**, 480–492 (2014)
6. Pagano, L., Reder, A., Rianna, G.: Processi di infiltrazione ed evaporazione nei terreni piroclastici illustrati attraverso la selezione di alcuni eventi rappresentativi. Rivista Italiana di Geotecnica **48**, 56–70 (2014)
7. Calabresi, G., Colleselli, F., Danese, D., Giani, G., Mancuso, C., Montrasio, L., Nocilla, A., Pagano, L., Reali, E., Sciotti, A.: Research study of the hydraulic behaviour of the Po river embankments. Can. Geotech. J. **50**, 947–960 (2013)
8. Pagano, L., Reder, A., Rianna, G.: Experiments to investigate the hydrological behaviour of volcanic covers, The Third Italian Workshop on Landslides (Naples, October 2013). Procedia Earth Planet Sci, Elsevier, doi: 10.1016/j.proeps.2014.06.013, 9, 14–22 (2014)
9. Pagano, L., Reder, A., Rianna, G.: Prediction of suction evolution of silty pyroclastic covers in flume tests and field monitoring, Paper describing predicted results for Round Robin Test of IWL2013 – The Third Italian Workshop on Landslides (Naples, October 2013). Procedia Earth Planet Sci. Elsevier, 9, 214–221 (2013)
10. Rianna, G., Pagano, L., Urciuoli, G.: A physical model to investigate the influence of atmospheric variables on soil suction in pyroclastic soils. In: Proceedings of the Second European Conference on Unsaturated Soils, E-UNSAT 2012: Unsaturated Soils: Research and Applications, Part 2, 221–227 (2012). doi: 10.1007/978-3-642-313431_28
11. Di Massa, G., Pagano, L., Pagano, S., Russo, M., Russo, R., Zingariello, C.: A mechanical slope for flowslide investigations, Lecture Notes in Engineering and Computer Science: Proceedings of The World Congress on Engineering 2014, WCE 2014, pp. 1376–1380, London. 2–4 July 2014

12. Pagano, S., Russo, R., Strano, S., Terzo, M.: Modelling and control of a hydraulically actuated shaking table employed for vibration absorber testing, ASME 2012. In: 11th Biennial Conference on Engineering systems Design and Analysis (ESDA) – Advanced Computational Mechanics – Nantes. July 2–4 2012
13. Pagano, S., Russo, R., Strano, S., Terzo, M.: Non-linear modelling and optimal control of a hydraulically actuated seismic isolator test rig. Mech. Syst. Signal Process. **35**(1–2), 255–278 (2013). doi:10.1016/j.ymssp.2012.09.002
14. Pagano, S., Russo, M., Strano, S., Terzo, M.: Seismic isolator test rig control using high-fidelity non-linear dynamic system modelling. Meccanica **49**(1), 169–179 (2014). doi:10.1007/s11012-013-9783-y
15. Rojas, J.C., Pagano, L., Zingariello, M.C., Mancuso, C., Giordano, G., Passeggio, G.: A new high capacity tensiometer: first results. CRC Press – Taylor & Francis Group, London I European Conference on Unsaturated Soils, pp. 205–211. Durham, 2–4 July 2008
16. Pagano, L., Reder, A., Rianna, G.: Calibration of TDRs and heat dissipation probes in pyroclastic soils, The Third Italian Workshop on Landslides (Naples, October 2013). Procedia Earth Planetary Sci.. Elsevier. **9**, 171–179 (2014). doi: 10.1016/j.proeps.2014.06.016